

1      **MitoChime: A Machine-Learning Pipeline for**  
2      **Detecting PCR-Induced Chimeras in**  
3      **Mitochondrial Illumina Reads**

4                          A Special Project Proposal  
5                          Presented to  
6                          the Faculty of the Division of Physical Sciences and Mathematics  
7                          College of Arts and Sciences  
8                          University of the Philippines Visayas  
9                          Miag-ao, Iloilo

10                         In Partial Fulfillment  
11                         of the Requirements for the Degree of  
12                         Bachelor of Science in Computer Science

13                         by

14                         Duranne Duran  
15                         Yvonne Lin  
16                         Daniella Pailden

17                         Adviser  
18                         Francis D. Dimzon, Ph.D.

19                         December 5, 2025

# **Contents**

21	<b>1 Introduction</b>	1
22	1.1 Overview . . . . .	1
23	1.2 Problem Statement . . . . .	3
24	1.3 Research Objectives . . . . .	4
25	1.3.1 General Objective . . . . .	4
26	1.3.2 Specific Objectives . . . . .	4
27	1.4 Scope and Limitations of the Research . . . . .	5
28	1.5 Significance of the Research . . . . .	6
29	<b>2 Review of Related Literature</b>	7
30	2.1 The Mitochondrial Genome . . . . .	7
31	2.1.1 Mitochondrial Genome Assembly . . . . .	8

32	2.2 PCR Amplification and Chimera Formation . . . . .	9
33	2.3 Existing Traditional Approaches for Chimera Detection . . . . .	10
34	2.3.1 UCHIME . . . . .	11
35	2.3.2 UCHIME2 . . . . .	12
36	2.3.3 CATch . . . . .	13
37	2.3.4 ChimPipe . . . . .	14
38	2.4 Machine Learning Approaches for Chimera and Sequence Quality	
39	Detection . . . . .	15
40	2.4.1 Feature-Based Representations of Genomic Sequences . . .	16
41	2.5 Synthesis of Chimera Detection Approaches . . . . .	17
42	<b>3 Research Methodology</b>	<b>20</b>
43	3.1 Research Activities . . . . .	20
44	3.1.1 Data Collection . . . . .	21
45	3.1.2 Feature Extraction Pipeline . . . . .	25
46	3.1.3 Machine Learning Model Development . . . . .	28
47	3.1.4 Model Benchmarking, Hyperparameter Optimization, and	
48	Evaluation . . . . .	29
49	3.1.5 Feature Importance and Interpretation . . . . .	30

50	3.1.6 Validation and Testing . . . . .	31
51	3.1.7 Documentation . . . . .	32
52	3.2 Calendar of Activities . . . . .	33
53	<b>4 Results and Discussion</b>	<b>34</b>
54	4.1 Descriptive Analysis of Features . . . . .	34
55	4.1.1 Univariate Distributions . . . . .	35
56	4.2 Baseline Classification Performance . . . . .	37
57	4.3 Effect of Hyperparameter Tuning . . . . .	38
58	4.4 Detailed Evaluation of Representative Models . . . . .	40
59	4.4.1 Confusion Matrices and Error Patterns . . . . .	41
60	4.4.2 ROC and Precision–Recall Curves . . . . .	42
61	4.5 Feature Importance and Biological Interpretation . . . . .	44
62	4.5.1 Permutation Importance of Individual Features . . . . .	44
63	4.5.2 Feature Family Importance . . . . .	45
64	4.6 Summary of Findings . . . . .	47

# <sup>65</sup> List of Figures

<sup>66</sup>	3.1 Process Diagram of Special Project . . . . .	21
<sup>67</sup>	4.1 Kernel density plots of six key features comparing clean and	
<sup>68</sup>	chimeric reads. . . . .	36
<sup>69</sup>	4.2 Test F1 of all baseline classifiers, showing that no single model	
<sup>70</sup>	clearly dominates and several achieve comparable performance. . .	38
<sup>71</sup>	4.3 Comparison of test F1 (left) and ROC–AUC (right) for baseline and	
<sup>72</sup>	tuned models. Hyperparameter tuning yields small but consistent	
<sup>73</sup>	gains, particularly for tree-based ensembles. . . . .	40
<sup>74</sup>	4.4 Confusion matrices for the four representative models on the held-	
<sup>75</sup>	out test set. All models show more false negatives (chimeric reads	
<sup>76</sup>	called clean) than false positives. . . . .	42
<sup>77</sup>	4.5 ROC (left) and precision–recall (right) curves for the four represen-	
<sup>78</sup>	tative models on the held-out test set. Tree-based ensembles cluster	
<sup>79</sup>	closely, with logistic regression performing slightly but consistently	
<sup>80</sup>	worse. . . . .	43

81	4.6 Permutation-based feature importance for four representative clas-	
82	sifiers. Clipping and k-mer composition features are generally the	
83	strongest predictors, whereas microhomology and other alignment	
84	metrics contribute minimally. . . . .	45
85	4.7 Aggregated feature family importance across four models. Clipping	
86	and k-mer compositional shifts are consistently the dominant con-	
87	tributors, while SA_structure, Micro_homology, and other features	
88	contribute minimally. . . . .	47

# **List of Tables**

89	2.1 Comparison of Chimera Detection Methods . . . . .	18
90	2.1 Comparison of Chimera Detection Methods . . . . .	18
91	3.1 Timetable of Activities . . . . .	33
92	3.1 Timetable of Activities . . . . .	33
92	4.1 Performance of baseline classifiers on the held-out test set. . . . .	38
93	4.1 Performance of baseline classifiers on the held-out test set. . . . .	38
93	4.2 Performance of tuned classifiers on the held-out test set. . . . .	39
93	4.2 Performance of tuned classifiers on the held-out test set. . . . .	39

<sup>94</sup> **Chapter 1**

<sup>95</sup> **Introduction**

<sup>96</sup> **1.1 Overview**

<sup>97</sup> The rapid advancement of next-generation sequencing (NGS) technologies has  
<sup>98</sup> transformed genomic research by enabling high-throughput and cost-effective  
<sup>99</sup> DNA analysis (Metzker, 2010). Among current platforms, Illumina sequencing  
<sup>100</sup> remains the most widely adopted, capable of producing millions of short reads  
<sup>101</sup> that can be assembled into reference genomes or analyzed for genetic variation  
<sup>102</sup> (Bentley et al., 2008; Glenn, 2011). Despite its high base-calling accuracy,  
<sup>103</sup> Illumina sequencing is prone to artifacts introduced during library preparation,  
<sup>104</sup> particularly polymerase chain reaction (PCR)-induced chimeras, which are ar-  
<sup>105</sup> tificial hybrid sequences that do not exist in the true genome (Judo, Wedel, &  
<sup>106</sup> Wilson, 1998).

<sup>107</sup> PCR chimeras form when incomplete extension products from one template

anneal to an unrelated DNA fragment and are extended, creating recombinant reads (Qiu et al., 2001). In mitochondrial genome assembly, such artifacts are especially problematic because the mitochondrial genome is small, circular, and often repetitive (Boore, 1999; Cameron, 2014). Even a small number of chimeric or misjoined reads can reduce assembly contiguity and introduce false junctions during organelle genome reconstruction (Dierckxsens, Mardulyn, & Smits, 2017; Hahn, Bachmann, & Chevreux, 2013; Jin et al., 2020). Existing assembly tools such as GetOrganelle and MITObim assume that input reads are largely free of such artifacts (Hahn et al., 2013; Jin et al., 2020). Consequently, undetected chimeras may produce fragmented assemblies or misidentified organellar boundaries. To ensure accurate reconstruction of mitochondrial genomes, a reliable method for detecting and filtering PCR-induced chimeras before assembly is essential.

This study focuses on mitochondrial sequencing data from the genus *Sardinella*, a group of small pelagic fishes widely distributed in Philippine waters. Among them, *Sardinella lemuru* (Bali sardinella) is one of the country's most abundant and economically important species, providing protein and livelihood to coastal communities (Labrador, Agmata, Palermo, Ravago-Gotanco, & Pante, 2021; Willette, Bognot, Mutia, & Santos, 2011). Accurate mitochondrial assemblies are critical for understanding its population genetics, stock structure, and evolutionary history. However, assembly pipelines often encounter errors or fail to complete due to undetected chimeric reads. To address this gap, this research introduces MitoChime, a machine learning pipeline designed to detect and filter PCR-induced chimeric reads using both alignment-based and sequence-derived statistical features. The tool aims to provide bioinformatics laboratories, partic-

<sub>133</sub> ularly the Philippine Genome Center Visayas (PGC Visayas), with an efficient  
<sub>134</sub> solution for improving mitochondrial genome reconstruction.

## <sub>135</sub> 1.2 Problem Statement

<sub>136</sub> While NGS technologies have revolutionized genomic data acquisition, the ac-  
<sub>137</sub> curacy of mitochondrial genome assembly remains limited by artifacts produced  
<sub>138</sub> during PCR amplification. These chimeric reads can distort assembly graphs and  
<sub>139</sub> cause misassemblies, with particularly severe effects in small, circular mitochon-  
<sub>140</sub> drial genomes (Boore, 1999; Cameron, 2014). Existing assembly pipelines such  
<sub>141</sub> as GetOrganelle, MITObim, and NOVOPlasty assume that sequencing reads are  
<sub>142</sub> free of such artifacts (Dierckxsens et al., 2017; Hahn et al., 2013; Jin et al., 2020).  
<sub>143</sub> At PGC Visayas, several mitochondrial assemblies have failed or yielded incom-  
<sub>144</sub> plete contigs despite sufficient coverage, suggesting that undetected chimeric reads  
<sub>145</sub> compromise assembly reliability. Meanwhile, existing chimera detection tools such  
<sub>146</sub> as UCHIME and VSEARCH were developed primarily for amplicon-based com-  
<sub>147</sub> munity analysis and rely heavily on reference or taxonomic comparisons (Edgar,  
<sub>148</sub> Haas, Clemente, Quince, & Knight, 2011; Rognes, Flouri, Nichols, Quince, &  
<sub>149</sub> Mahé, 2016). These approaches are unsuitable for single-species organellar data,  
<sub>150</sub> where complete reference genomes are often unavailable. Therefore, there is a  
<sub>151</sub> pressing need for a reference-independent, data-driven tool capable of detecting  
<sub>152</sub> and filtering PCR-induced chimeras in mitochondrial sequencing datasets.

<sub>153</sub> **1.3 Research Objectives**

<sub>154</sub> **1.3.1 General Objective**

<sub>155</sub> This study aims to develop and evaluate a machine learning-based pipeline (Mi-  
<sub>156</sub> toChime) that detects PCR-induced chimeric reads in *Sardinella lemuru* mito-  
<sub>157</sub> chondrial sequencing data in order to improve the quality and reliability of down-  
<sub>158</sub> stream mitochondrial genome assemblies.

<sub>159</sub> **1.3.2 Specific Objectives**

<sub>160</sub> Specifically, the study aims to:

- <sub>161</sub> 1. construct simulated *Sardinella lemuru* Illumina paired-end datasets contain-  
<sub>162</sub> ing both clean and PCR-induced chimeric reads,
- <sub>163</sub> 2. extract alignment-based and sequence-based features such as k-mer compo-  
<sub>164</sub> sition, junction complexity, and split-alignment counts from both clean and  
<sub>165</sub> chimeric reads,
- <sub>166</sub> 3. train, validate, and compare supervised machine-learning models for classi-  
<sub>167</sub> fying reads as clean or chimeric,
- <sub>168</sub> 4. determine feature importance and identify indicators of PCR-induced  
<sub>169</sub> chimerism,
- <sub>170</sub> 5. integrate the optimized classifier into a modular and interpretable pipeline  
<sub>171</sub> deployable on standard computing environments at PGC Visayas.

## 172 1.4 Scope and Limitations of the Research

173 This study focuses on detecting PCR-induced chimeric reads in Illumina paired-  
174 end mitochondrial sequencing data from *Sardinella lemuru*. The decision to re-  
175 strict the taxonomic scope to a single species is based on four considerations: to  
176 limit interspecific variation in mitochondrial genome size, GC content, and repeti-  
177 tive regions so that differences in read patterns can be attributed more directly to  
178 PCR-induced chimerism; to align the analysis with relevant *S. lemuru* sequencing  
179 projects at PGC Visayas; to take advantage of the availability of *S. lemuru* mito-  
180 chondrial assemblies and raw datasets in public repositories such as the National  
181 Center for Biotechnology Information (NCBI), which facilitates reference selection  
182 and benchmarking; and to develop a tool that directly supports local studies on  
183 *S. lemuru* population structure and fisheries management.

184 The study emphasizes `wgsim`-based simulations and selected empirical mito-  
185 chondrial datasets from *S. lemuru*. It excludes naturally occurring chimeras, nu-  
186 clear mitochondrial pseudogenes (NUMTs), and large-scale assembly rearrange-  
187 ments in nuclear genomes. Feature extraction is restricted to low-dimensional  
188 alignment and sequence statistics, such as k-mer frequency profiles, GC content,  
189 read length, soft and hard clipping metrics, split-alignment counts, and map-  
190 ping quality, rather than high-dimensional deep learning embeddings. This de-  
191 sign keeps model behaviour interpretable and ensures that the pipeline can be  
192 run on standard workstations at PGC Visayas. Testing on long-read platforms  
193 (e.g., Nanopore, PacBio) and other taxa is outside the scope of this project; the  
194 implemented pipeline is evaluated only on short-read *S. lemuru* datasets.

195 Other limitations in this study include the following: simulations with varying

196 error rates were not performed, so the effect of different sequencing errors on model  
197 performance remains unexplored; alternative parameter settings, including k-mer  
198 lengths and microhomology window sizes, were not systematically tested, which  
199 could affect the sensitivity of both k-mer and microhomology feature detection as  
200 well as the identification of chimeric junctions; and the machine-learning models  
201 rely on supervised training with labeled examples, which may limit their ability  
202 to detect novel or unexpected chimeric patterns.

## 203 1.5 Significance of the Research

204 This research provides both methodological and practical contributions to mito-  
205 chondrial genomics and bioinformatics. First, MitoChime detects PCR-induced  
206 chimeric reads prior to genome assembly, with the goal of improving the con-  
207 tiguity and correctness of *Sardinella lemuru* mitochondrial assemblies. Second,  
208 it replaces informal manual curation with a documented workflow, improving au-  
209 tomation and reproducibility. Third, the pipeline is designed to run on computing  
210 infrastructures commonly available in regional laboratories, enabling routine use  
211 at facilities such as PGC Visayas. Finally, more reliable mitochondrial assemblies  
212 for *S. lemuru* provide a stronger basis for downstream applications in the field of  
213 fisheries and genomics.

<sup>214</sup> **Chapter 2**

<sup>215</sup> **Review of Related Literature**

<sup>216</sup> This chapter presents an overview of the literature relevant to the study. It  
<sup>217</sup> discusses the biological and computational foundations underlying mitochondrial  
<sup>218</sup> genome analysis and assembly, as well as existing tools, algorithms, and techniques  
<sup>219</sup> related to chimera detection and genome quality assessment. The chapter aims to  
<sup>220</sup> highlight the strengths, limitations, and research gaps in current approaches that  
<sup>221</sup> motivate the development of the present study.

<sup>222</sup> **2.1 The Mitochondrial Genome**

<sup>223</sup> Mitochondrial genome (mtDNA) is a small, typically circular molecule found in  
<sup>224</sup> most eukaryotes. It encodes essential genes involved in oxidative phosphorylation  
<sup>225</sup> and energy metabolism. Because of its conserved structure, mtDNA has become  
<sup>226</sup> a valuable genetic marker for studies in population genetics and phylogenetics  
<sup>227</sup> (Anderson et al., 1981; Boore, 1999). In animal species, the mitochondrial genome

ranges from 15–20 kilobase and contains 13 protein-coding genes, 22 tRNAs, and two rRNAs arranged compactly without introns (Gray, 2012). In comparison to nuclear DNA, the ratio of the number of copies of mtDNA is higher and has simple organization which make it particularly suitable for genome sequencing and assembly studies (Dierckxsens et al., 2017).

### 2.1.1 Mitochondrial Genome Assembly

Mitochondrial genome assembly refers to the reconstruction of the complete mitochondrial DNA (mtDNA) sequence from raw or fragmented sequencing reads. It is conducted to obtain high-quality, continuous representations of the mitochondrial genome that can be used for a wide range of analyses, including species identification, phylogenetic reconstruction, evolutionary studies, and investigations of mitochondrial diseases. Because mtDNA evolves rapidly, its assembled sequence provides valuable insights into population structure, lineage divergence, and adaptive evolution across taxa (Boore, 1999). Compared to nuclear genome assembly, assembling the mitochondrial genome is often considered more straightforward but still encounters technical challenges such as the formation of chimeric reads. Commonly used tools for mitogenome assembly such as GetOrganelle and MITObim operate under the assumption of organelle genome circularity, and are vulnerable when chimeric reads disrupt this circular structure, resulting in assembly errors (Hahn et al., 2013; Jin et al., 2020).

## **248    2.2 PCR Amplification and Chimera Formation**

**249** PCR plays an important role in NGS library preparation, as it amplifies target  
**250** DNA fragments for downstream analysis. However as previously mentioned, the  
**251** amplification process can also introduce chimeric reads which compromises the  
**252** quality of the input reads supplied to sequencing or assembly workflows. Chimeras  
**253** typically arise when incomplete extension occurs during a PCR cycle. This causes  
**254** the DNA polymerase to switch from one template to another and generate hy-  
**255** brid recombinant molecules (Judo et al., 1998). Artificial chimeras are produced  
**256** through such amplification errors, whereas biological chimeras occur naturally  
**257** through genomic rearrangements or transcriptional events.

**258** In the context of amplicon-based sequencing, the presence of chimeras can in-  
**259** flate estimates of genetic or microbial diversity and may cause misassemblies dur-  
**260** ing genome reconstruction. Qin et al. (2023) has reported that chimeric sequences  
**261** may account for more than 10% of raw reads in amplicon datasets. This artifact  
**262** tends to be most prominent among rare operational taxonomic units (OTUs) or  
**263** singletons, which are sometimes misinterpreted as novel diversity, further caus-  
**264** ing the complication of microbial diversity analyses (Gonzalez, Zimmermann, &  
**265** Saiz-Jimenez, 2004). As such, determining and minimizing PCR-induced chimera  
**266** formation is vital for improving the quality of mitochondrial genome assemblies,  
**267** and ensuring the reliability of amplicon sequencing data.

268 **2.3 Existing Traditional Approaches for Chimera**

269 **Detection**

270 Several computational tools have been developed to identify chimeric sequences in  
271 NGS datasets. These tools generally fall into two categories: reference-based and  
272 de novo approaches. Reference-based chimera detection, also known as database-  
273 dependent detection, is one of the earliest and most widely used computational  
274 strategies for identifying chimeric sequences in amplicon-based community studies.  
275 These methods rely on the comparison of each query sequence against a curated,  
276 high-quality database of known, non-chimeric reference sequences (Edgar et al.,  
277 2011).

278 On the other hand, the de novo chimera detection, also referred to as reference-  
279 free detection, represents an alternative computational paradigm that identifies  
280 chimeric sequences without reliance on external reference databases. This method  
281 infer chimeras based on internal relationships among the sequences present within  
282 the dataset itself, making it particularly advantageous in studies of under explored  
283 or taxonomically diverse communities where comprehensive reference databases  
284 are unavailable or incomplete (Edgar, 2016; Edgar et al., 2011). The underlying  
285 assumption on this method is that during PCR, true biological sequences are  
286 generally more abundant as they are amplified early and dominate the read pool,  
287 whereas chimeric sequences appear later and are generally less abundant. The  
288 de novo approach leverage this abundance hierarchy, treating the most abundant  
289 sequences as supposed parents and testing whether less abundant sequences can  
290 be reconstructed as mosaics of these templates. Compositional and structural  
291 similarity are also evaluated to check whether different regions of a candidate

292 sequence correspond to distinct high-abundance sequences.

293 In practice, many modern bioinformatics pipelines combine both paradigms  
294 sequentially: an initial de novo step identifies dataset-specific chimeras, followed  
295 by a reference-based pass that removes remaining artifacts relative to established  
296 databases (Edgar, 2016). These two methods of detection form the foundation of  
297 tools such as UCHIME and later UCHIME2.

### 298 2.3.1 UCHIME

299 UCHIME is one of the most widely used computational tools for detecting chimeric  
300 sequences in amplicon sequencing data, as it serves as a critical quality control  
301 step to prevent the misinterpretation of PCR artifacts as novel biological diversity.  
302 The algorithm operates by searching for a model ( $M$ ) where a query ( $Q$ ) sequence  
303 can be perfectly explained as a combination of two parent sequences, denoted as  
304  $A$  and  $B$  (Edgar et al., 2011).

305 In reference mode, UCHIME divides the query into four chunks and maps  
306 them to a trusted chimeric-free database to identify candidate parents. It then  
307 constructs a three-way alignment to calculate a score based on “votes.” A “Yes”  
308 vote indicates the query aligns with parent  $A$  in one region and parent  $B$  in an-  
309 other, while a “No” vote penalizes the score if the query diverges from the expected  
310 chimeric model. In de novo mode, the algorithm operationalizes the abundance  
311 skew principle described in Section 2.3. Instead of using an external database,  
312 UCHIME dynamically treats the sample’s own high-abundance sequences as a  
313 reference database, testing if lower-abundance sequences can be reconstructed as

314 mosaics of these internal ancestors (Edgar et al., 2011).

315 Despite its high sensitivity, UCHIME has inherent limitations rooted in  
316 sequence divergence and database quality. The algorithm struggles to detect  
317 chimeras formed from parents that are very closely related, specifically when the  
318 sequence divergence between parents is less than roughly 0.8%, as the signal-to-  
319 noise ratio becomes too low to distinguish a crossover event from sequencing error  
320 (Edgar et al., 2011). Furthermore, in reference mode, the accuracy is strictly  
321 bound by the completeness of the database; if true parents are absent, the tool  
322 may fail to identify the chimera or produce false positives. Similarly, the de novo  
323 mode relies on the assumption that parents are present and sufficiently more  
324 abundant in the sample, which may not hold true in unevenly amplified samples  
325 or complex communities.

### 326 2.3.2 UCHIME2

327 Building upon the original algorithm, UCHIME2 was developed to address the  
328 nuances of high-resolution amplicon sequencing. A key contribution of the  
329 UCHIME2 study was the critical re-evaluation of chimera detection benchmarks.  
330 In the UCHIME2 paper (Edgar, 2016) and the UCHIME in practice website  
331 (Edgar, n.d), the author has noted that the accuracy results reported in the  
332 original UCHIME paper were “highly over-optimistic” because they relied on  
333 unrealistic benchmark designs where parent sequences were assumed to be 100%  
334 known and present. UCHIME2 introduced more rigorous testing (the CHSIMA  
335 benchmark), revealing that “fake models,” where a valid biological sequence  
336 perfectly mimics a chimera of two other valid sequences, are far more common

337 than previously assumed. This discovery suggests that error-free detection is  
338 impossible in principle (Edgar, 2016). Another notable improvement is the in-  
339 troduction of multiple application-specific modes that allow users to tailor the  
340 algorithm’s performance to the characteristics of their datasets. The following  
341 parameter presets: denoised, balanced, sensitive, specific, and high-confidence,  
342 enable researchers to optimize the balance between sensitivity and specificity  
343 according to the goals of their analysis.

344 However despite these advancements, the practical application of UCHIME2  
345 requires caution. The author explicitly advises against using UCHIME2 as  
346 a stand-alone tool in standard OTU clustering or denoising pipelines. Using  
347 UCHIME2 as an independent filtering step in these workflows is discouraged, as  
348 it often results in significantly higher error rates, increasing both false positives  
349 (discarding valid sequences) and false negatives (retaining chimeras) (Edgar,  
350 2016).

### 351 2.3.3 CATch

352 As previously mentioned, UCHIME (Edgar et al., 2011) relied on alignment-based  
353 sequences in amplicon data. However, researchers soon observed that different al-  
354 gorithms often produced inconsistent predictions. A sequence might be identified  
355 as chimeric by one tool but classified as non-chimeric by another, resulting in  
356 unreliable filtering outcomes across studies.

357 To address these inconsistencies, Mysara, Saeys, Leys, Raes, and Monsieurs  
358 (2015) developed the Classifier for Amplicon Tool Chimeras (CATCh), which rep-

359 resents the first ensemble machine learning system designed for chimera detection  
360 in 16S rRNA amplicon sequencing. Rather than depending on a single detec-  
361 tion strategy, CATCh integrates the outputs of several established tools, includ-  
362 ing UCHIME, ChimeraSlayer, DECIPHER, Pintail, and Perseus. The individual  
363 scores and binary decisions generated by these tools are used as input features for  
364 a supervised learning model. The algorithm employs a Support Vector Machine  
365 (SVM) with a Pearson VII Universal Kernel (PUK) to determine optimal weight-  
366 ings among the input features and to assign each sequence a probability of being  
367 chimeric.

368 Benchmarking in both reference-based and de novo modes demonstrated signif-  
369 icant performance improvements. CATCh achieved sensitivities of approximately  
370 85 percent in reference-based mode and 92 percent in de novo mode, with corre-  
371 sponding specificities of approximately 96 percent and 95 percent. These results  
372 indicate that CATCh detected 7 to 12 percent more chimeras than any individual  
373 algorithm while maintaining high precision.

### 374 **2.3.4 ChimPipe**

375 Among the available tools for chimera detection, ChimPipe is a pipeline developed  
376 to identify chimeric sequences such as biological chimeras. It uses both discordant  
377 paired-end reads and split-read alignments to improve the accuracy and sensitivity  
378 of detecting biological chimeras (Rodriguez-Martin et al., 2017). By combining  
379 these two sources of information, ChimPipe achieves better precision than meth-  
380 ods that depend on a single type of indicator.

381        The pipeline works with many eukaryotic species that have available genome  
382        and annotation data (Rodriguez-Martin et al., 2017). It can also predict multiple  
383        isoforms for each gene pair and identify breakpoint coordinates that are useful  
384        for reconstructing and verifying chimeric transcripts. Tests using both simulated  
385        and real datasets have shown that ChimPipe maintains high accuracy and reliable  
386        performance.

387        ChimPipe lets users adjust parameters to fit different sequencing protocols or  
388        organism characteristics. Experimental results have confirmed that many chimeric  
389        transcripts detected by the tool correspond to functional fusion proteins, demon-  
390        strating its utility for understanding chimera biology and its potential applications  
391        in disease research (Rodriguez-Martin et al., 2017).

## 392        **2.4 Machine Learning Approaches for Chimera 393                          and Sequence Quality Detection**

394        Traditional chimera detection tools rely primarily on heuristic or alignment-based  
395        rules. Recent advances in machine learning (ML) have demonstrated that models  
396        trained on sequence-derived features can effectively capture compositional and  
397        structural patterns in biological sequences. Although most existing ML systems  
398        such as those used for antibiotic resistance prediction, taxonomic classification,  
399        or viral identification are not specifically designed for chimera detection, they  
400        highlight how data-driven models can outperform similarity-based heuristics by  
401        learning intrinsic sequence signatures. In principle, ML frameworks can integrate  
402        indicators such as k-mer frequencies, GC-content variation and split-alignment

403 metrics to identify subtle anomalies that may indicate a chimeric origin (Arango  
404 et al., 2018; Liang, Bible, Liu, Zou, & Wei, 2020; Ren et al., 2020).

405 **2.4.1 Feature-Based Representations of Genomic Se-  
406 quences**

407 Feature extraction converts DNA sequences into numerical representations suit-  
408 able for machine-learning models. One approach is k-mer frequency analysis,  
409 which counts short nucleotide sequences within a read (Vervier, Mahé, Tournoud,  
410 Veyrieras, & Vert, 2015). High-frequency k-mers, including simple repeats such  
411 as “AAAAAA,” can highlight repetitive or unusual regions that may occur near  
412 chimeric junctions. Comparing k-mer patterns across adjacent parts of a read can  
413 help identify such regions, while GC content provides an additional descriptor of  
414 local sequence composition (Ren et al., 2020).

415 Alignment-derived features further inform junction detection. Long-read tools  
416 such as Sniffles (Sedlazeck et al., 2018) use split alignments to locate breakpoints  
417 across extended sequences, whereas short-read aligners like Minimap2 (Li, 2018)  
418 report supplementary and secondary alignments that indicate local discontinu-  
419 ities. Split alignments, where parts of a read map to different regions, can reveal  
420 template-switching events. These features complement k-mer profiles and en-  
421 hance detection of potentially chimeric reads, even in datasets with incomplete  
422 references.

423 Microhomology, or short sequences shared between adjacent segments, is an-  
424 other biologically meaningful feature. Its length, typically a few to tens of base

425 pairs, has been linked to microhomology-mediated repair and template-switching  
426 mechanisms (Sfeir & Symington, 2015). In PCR-induced chimeras, short iden-  
427 tical sequences at junctions provide a clear signature of chimerism. Measuring  
428 the longest exact overlap at each breakpoint complements k-mer and alignment  
429 features and helps identify reads that are potentially chimeric.

## 430 2.5 Synthesis of Chimera Detection Approaches

431 To provide an integrated overview of the literature discussed in this chapter, Ta-  
432 ble 2.1 summarizes the major chimera detection studies, their methodological  
433 approaches, and their known limitations.

Table 2.1: Comparison of Chimera Detection Methods

Methods	Approach	Limitations
<b>Reference-based Chimera Detection</b>	Compares query sequences against curated, non-chimeric reference databases; identifies mosaic sequences by evaluating similarity to known templates.	Depends heavily on completeness and quality of reference databases; often fails when novel taxa or missing parent sequences are present; reduced accuracy for low-divergence chimeras.
<b>De novo Chimera Detection</b>	Identifies chimeras using only internal dataset relationships; relies on abundance patterns and compositional similarity; reconstructs sequences as mosaics of high-abundance parents.	Assumes true sequences are more abundant—fails when amplification bias distorts abundance; struggles with evenly abundant parental sequences; can misclassify highly similar true variants.
<b>UCHIME</b>	Alignment-based chimera detection; segments query sequence, identifies parent candidates, performs 3-way alignment, and computes chimera scores; supports both reference-based and de novo modes.	Accuracy inflated in original benchmarks; suffers under incomplete databases; poor performance on low-divergence chimeras; sensitive to sequencing errors; misclassifies when parents are missing.
<b>UCHIME2</b>	Improved initial UCHIME benchmarking; offers multiple sensitivity/specificity modes; more robust with incomplete references; higher sensitivity.	Cannot achieve perfect accuracy due to “perfect fake models”; genuine variants may be indistinguishable from artificial recombinants; theoretical detection limit remains.
<b>CATCh</b>	First ML ensemble tool for 16S chimera detection; integrates outputs of UCHIME, ChimeraSlayer, DECI-PHER, Pintail, Perseus via SVM classifier; significantly improves sensitivity and specificity.	Depends on performance of underlying tools; ML model limited to features they output; ensemble can still misclassify in datasets with extreme novelty or low coverage.
<b>ChimPipe</b>	Pipeline for detecting fusion genes and transcript-derived chimeras in RNA-seq; uses discordant paired-end reads and split-alignments; predicts isoforms and breakpoint coordinates.	Designed for RNA-seq, not amplicons; needs high-quality genome and annotation; computationally heavier; limited to organisms with reference genomes.

434 Across existing studies, no single approach reliably detects all forms of chimeric  
435 sequences, particularly those generated by PCR-induced template switching in  
436 mitochondrial genomes. Reference-based tools perform poorly when parental se-  
437 quences are absent; de novo methods rely strongly on abundance assumptions;  
438 alignment-based systems show reduced sensitivity to low-divergence chimeras; and  
439 ensemble methods inherit the limitations of their component algorithms. RNA-  
440 seq-oriented pipelines likewise do not generalize well to organelle data. Although  
441 machine learning approaches offer promising feature-based detection, they are  
442 rarely applied to mitochondrial genomes and are not trained specifically on PCR-  
443 induced organelle chimeras. These limitations indicate a clear research gap: the  
444 need for a specialized, feature-driven classifier tailored to mitochondrial PCR-  
445 induced chimeras that integrates k-mer composition, split-alignment signals, and  
446 microhomology features to achieve more accurate detection than current heuristic  
447 or alignment-based tools.

# <sup>448</sup> Chapter 3

## <sup>449</sup> Research Methodology

<sup>450</sup> This chapter outlines the steps involved in completing the study, including data  
<sup>451</sup> gathering, generating simulated mitochondrial Illumina reads, preprocessing and  
<sup>452</sup> indexing the data, developing a feature extraction pipeline to extract key features,  
<sup>453</sup> applying machine learning algorithms for chimera detection, and validating and  
<sup>454</sup> comparing model performance.

### <sup>455</sup> 3.1 Research Activities

<sup>456</sup> As illustrated in Figure 3.1, this study carried out a sequence of procedures to  
<sup>457</sup> detect PCR-induced chimeric reads in mitochondrial genomes. The process began  
<sup>458</sup> with collecting a mitochondrial reference sequence of *Sardinella lemuru* from the  
<sup>459</sup> National Center for Biotechnology Information (NCBI) database, which was used  
<sup>460</sup> as a reference for generating simulated clean and chimeric reads. These reads  
<sup>461</sup> were subsequently indexed and mapped. The resulting collections then passed

462 through a feature extraction pipeline that extracted k-mer profiles, supplementary  
463 alignment (SA) features, and microhomology information to prepare the data for  
464 model construction. The machine learning model was trained using the processed  
465 input, and its precision and accuracy were assessed. It underwent tuning until it  
466 reached the desired performance threshold, after which it proceeded to validation  
467 and will undergo testing.

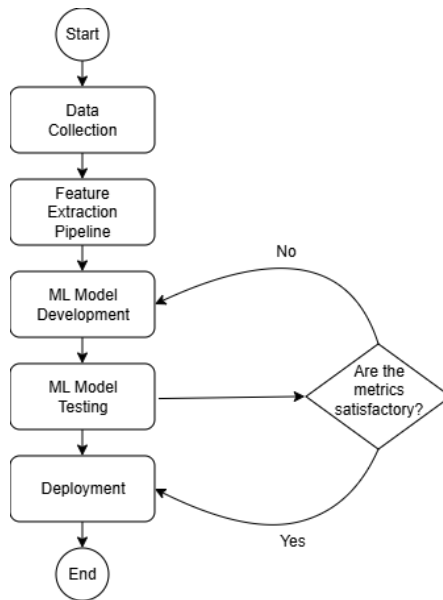


Figure 3.1: Process Diagram of Special Project

### 468 3.1.1 Data Collection

469 The mitochondrial genome reference sequence of *S. lemuru* was obtained from the  
470 NCBI database (accession number NC\_039553.1) in FASTA format. This sequence  
471 served as the basis for generating simulated reads for model development.

472 This step was scheduled to begin in the first week of November 2025 and  
473 expected to be completed by the end of that week, with a total duration of ap-

474 proximately one (1) week.

## 475 Data Preprocessing

476 To reduce manual repetition, all steps in the simulation and preprocessing pipeline  
477 were executed using a custom script in Python (Version 3.11). The script runs  
478 each stage, including read simulation, reference indexing, mapping, and alignment  
479 processing, in a fixed sequence.

480 Sequencing data were simulated from the NCBI reference genome using `wgsim`  
481 (Version 1.13). First, a total of 10,000 paired-end fragments were simulated,  
482 producing 20,000 reads (10,000 forward and 10,000 reverse) from the the original  
483 reference (`original_reference.fasta`) and and designated as clean reads using  
484 the command:

```
485 wgsim -1 150 -2 150 -r 0 -R 0 -X 0 -e 0.001 -N 10000 \
486     original_reference.fasta ref1.fastq ref2.fastq
```

487 The command parameters are as follows:

- 488 • `-1` and `-2`: read lengths of 150 base pairs for each paired-end read.
- 489 • `-r`, `-R`, `-X`: mutation rate, fraction of indels, and indel extension probability,  
490 all set to a default value of 0.
- 491 • `-e`: base error rate, set to 0.001 to simulate realistic sequencing errors.
- 492 • `-N`: number of read pairs, set to 10,000.

493 Chimeric sequences were then generated from the same NCBI reference using a  
494 separate Python script. Two non-adjacent segments were randomly selected such  
495 that their midpoint distances fell within specified minimum and maximum thresh-  
496 olds. The script attempts to retain microhomology, or short identical sequences  
497 at segment junctions, to mimic PCR-induced template switching. The resulting  
498 chimeras were written to `chimera_reference.fasta`, with headers recording seg-  
499 ment positions and microhomology length. The `chimera_reference.fasta` was  
500 processed with `wgsim` to simulate 10,000 paired-end fragments, generating 20,000  
501 chimeric reads (10,000 forward reads in `chimeric1.fastq` and 10,000 reverse reads  
502 in `chimeric2.fastq`) using the command format.

503 Next, a `minimap2` index of the reference genome was created using:

```
504 minimap2 -d ref.mmi original_reference.fasta
```

505 Minimap2 (Version 2.28) is a tool used to map reads to a reference genome.  
506 The index `ref.mmi` of the original reference sequence is required by `minimap2` for  
507 efficient read mapping. Mapping allows extraction of alignment features from each  
508 read, which were used as input for the machine learning model. The simulated  
509 clean and chimeric reads were then mapped to the reference index as follows:

```
510 minimap2 -ax sr -t 8 ref.mmi ref1.fastq ref2.fastq > clean.sam
```

```
511 minimap2 -ax sr -t 8 ref.mmi \  
512 chimeric1.fastq chimeric2.fastq > chimeric.sam
```

513 Here, `-ax sr` specifies short-read alignment mode, and `-t 8` uses 8 CPU

514 threads. The resulting clean and chimeric SAM files contain the alignment posi-  
515 tions of each read relative to the original reference genome.

516 The SAM files were then converted to BAM format, sorted, and indexed using

517 `samtools` (Version 1.20):

```
518 samtools view -bS clean.sam -o clean.bam  
519 samtools view -bS chimeric.sam -o chimeric.bam  
520  
521 samtools sort clean.bam -o clean.sorted.bam  
522 samtools index clean.sorted.bam  
523  
524 samtools sort chimeric.bam -o chimeric.sorted.bam  
525 samtools index chimeric.sorted.bam
```

526 BAM files are the compressed binary version of SAM files, which enables faster  
527 processing and reduced storage. Sorting arranges reads by genomic coordinates,  
528 and indexing allows detection of SA as a feature for the machine learning model.

529 The total number of simulated reads was expected to be 40,000. The final col-  
530 lection of reads contained 19,984 clean reads and 20,000 chimeric reads (39,984 en-  
531 tries in total), providing a roughly balanced distribution between the two classes.  
532 After alignment with `minimap2`, only 19,984 clean reads remained because un-  
533 mapped reads were not included in the BAM file. Some sequences failed to align  
534 due to the 5% error rate defined during `wgsim` simulation, which produced mis-  
535 matches that caused certain reads to fall below the aligner's matching threshold.

536 This whole process is scheduled to start in the second week of November 2025

537 and is expected to be completed by the last week of November 2025, with a total  
538 duration of approximately three (3) weeks.

### 539 3.1.2 Feature Extraction Pipeline

540 This stage directly follows the previous alignment phase, utilizing the resulting  
541 BAM files (specifically `chimeric.sorted.bam` and `clean.sorted.bam`). A custom  
542 Python script was created to efficiently process each primary-mapped read to  
543 extract the necessary set of analytical features, which are then compiled into a  
544 structured feature matrix in TSV format. The pipeline's core functionality relies  
545 on libraries, namely `Pysam` (Version 0.22) for the robust parsing of BAM structures  
546 and `NumPy` (Version 1.26) for array operations and computations. The pipeline  
547 focuses on three principal features that collectively capture biological signatures  
548 associated with PCR-induced chimeras: (1) Supplementary alignment flag (SA  
549 count), (2) k-mer composition difference, and (3) microhomology.

#### 550 Supplementary Alignment Flag

551 Split-alignment information was derived from the `SA` (Supplementary Alignment)  
552 tag embedded in each primary read of the BAM file. This tag is typically asso-  
553 ciated with reads that map to multiple genomic locations, suggesting a chimeric  
554 structure. To extract this information, the script first checked whether the read  
555 carried an `SA:Z` tag. If present, the tag string was parsed using the function  
556 `parse_sa_tag`, yielding a structure for each alignment containing the reference  
557 name, mapped position, strand, mapping quality, and number of mismatches.

558 After parsing, the function `sa_feature_stats` was applied to establish the fun-  
559 damental split indicators, `has_sa` and `sa_count`. Along with these initial counts,  
560 the function synthesized a summarization by aggregating metrics related to the  
561 structure and reliability of the split alignments.

## 562 K-mer Composition Difference

563 Chimeric reads often comprise fragments from distinct genomic regions, resulting  
564 in a compositional discontinuity between segments. Comparing k-mer frequency  
565 profiles between the left and right halves of a read allows for the detection of such  
566 abrupt compositional shifts, independent of alignment information.

567 The script implemented this by inferring a likely junction breakpoint using  
568 the function `infer_breakpoints`, prioritizing the boundaries defined by soft-  
569 clipping operations in the CIGAR string. If no clipping was present, the midpoint  
570 of the alignment or the read length was utilized as a fallback. The read sequence  
571 was then divided into left and right segments at this inferred breakpoint, and  
572 k-mer frequency profiles ( $k = 5$ ) were generated for both halves, ignoring any  
573 k-mers containing ambiguous 'N' bases. The resulting k-mer frequency vectors  
574 will be normalized and compared using the functions `cosine_difference` and  
575 `js_divergence`.

## 576 Microhomology

577 The workflow for extracting the microhomology feature also started by utilizing  
578 the `infer_breakpoints` similar to the k-mer workflow. Once a breakpoint was es-

579 established, the script scanned a  $\pm 40$  base pair window surrounding the breakpoint  
580 and used the function `longest_suffix_prefix_overlap` to identify the longest  
581 exact suffix-prefix overlap between the left and right read segments. This overlap,  
582 which represents consecutive bases shared at the junction, was recorded as the  
583 `microhomology_length` in the dataset. The 40-base pair window was chosen to  
584 ensure that short shared sequences at or near the breakpoint were captured, with-  
585 out including distant sequences that are unrelated. Additionally, the GC content  
586 of the overlapping sequence was calculated using the function `gc_content`, which  
587 counts guanine (G) and cytosine (C) bases within the detected microhomology  
588 and divides by the total length, yielding a proportion between 0 and 1, and was  
589 stored under the `microhomology_gc` attribute. Short microhomologies, typically  
590 3-20 base pairs in length, are recognized signatures of PCR-induced template  
591 switching (Peccoud et al., 2018).

592 A k-mer length of 6 was used to capture patterns within the same 40-base pair  
593 window surrounding each breakpoint. These profiles complement microhomology  
594 measurements and help identify junctions that are potentially chimeric.

595 To ensure correctness and adherence to best practices, bioinformatics experts  
596 at the PGC Visayas will be consulted to validate the pipeline design, feature  
597 extraction logic, and overall data integrity. This stage of the study was scheduled  
598 to begin in the third week of November 2025 and conclude by the first week  
599 of December 2025, with an estimated total duration of approximately three (3)  
600 weeks.

601    **3.1.3 Machine Learning Model Development**

602    After feature extraction, the per-read feature matrices for clean and chimeric  
603    reads were merged into a single dataset. Each row corresponded to one paired-  
604    end read, and columns encoded alignment-structure features (e.g., supplementary  
605    alignment count and spacing between segments), CIGAR-derived soft-clipping  
606    statistics (e.g., left and right soft-clipped length, total clipped bases), k-mer com-  
607    position discontinuity between read segments, and microhomology descriptors  
608    near candidate junctions. The resulting feature set was restricted to quantities  
609    that can be computed from standard BAM/FASTQ files in typical mitochondrial  
610    sequencing workflows.

611    The labelled dataset was randomly partitioned into training (80%) and test  
612    (20%) subsets using stratified sampling to preserve the 1:1 ratio of clean to  
613    chimeric reads. Model development and evaluation were implemented in Python  
614    (Version 3.11) using the `scikit-learn`, `xgboost`, `lightgbm`, and `catboost` li-  
615    braries. A broad panel of classification algorithms was then benchmarked on the  
616    training data to obtain a fair comparison of different model families under identical  
617    feature conditions. The panel included: a trivial dummy classifier, L2-regularized  
618    logistic regression, a calibrated linear support vector machine (SVM),  $k$ -nearest  
619    neighbours, Gaussian Naïve Bayes, decision-tree ensembles (Random Forest, Ex-  
620    tremely Randomized Trees, and Bagging with decision trees), gradient boosting  
621    methods (Gradient Boosting, XGBoost, LightGBM, and CatBoost), and a shallow  
622    multilayer perceptron (MLP).

623    For each model, five-fold stratified cross-validation was performed on the train-  
624    ing set. In every fold, four-fifths of the data were used for fitting and the remaining

625 one-fifth for validation. Mean cross-validation accuracy, precision, recall, F1-score  
626 for the chimeric class, and area under the receiver operating characteristic curve  
627 (ROC–AUC) were computed to summarize performance and rank candidate meth-  
628 ods. This baseline screen allowed comparison of linear, probabilistic, neural, and  
629 ensemble-based approaches and identified tree-based ensemble and boosting mod-  
630 els as consistently strong performers relative to simpler baselines.

631 **3.1.4 Model Benchmarking, Hyperparameter Optimiza-  
632 tion, and Evaluation**

633 Model selection and refinement proceeded in two stages. First, the cross-validation  
634 results from the broad panel were used to identify a subset of competitive mod-  
635 els for more detailed optimization. Specifically, ten model families were carried  
636 forward: L2-regularized logistic regression, calibrated linear SVM, Random For-  
637 est, ExtraTrees, Gradient Boosting, XGBoost, LightGBM, CatBoost, Bagging  
638 with decision trees, and a shallow MLP. This subset spans both linear and non-  
639 linear decision boundaries, but emphasizes ensemble and boosting methods, which  
640 showed superior F1 and ROC–AUC in the initial benchmark.

641 Second, hyperparameter optimization was conducted for each of the ten se-  
642 lected models using randomized search with five-fold stratified cross-validation  
643 (`RandomizedSearchCV`). For tree-based ensembles, the search space included the  
644 number of trees, maximum depth, minimum samples per split and leaf, and the  
645 fraction of features considered at each split. For boosting methods, key hyper-  
646 parameters such as the number of boosting iterations, learning rate, tree depth,  
647 subsampling rate, and column subsampling rate were tuned. For the MLP, the

648 number and size of hidden layers, learning rate, and  $L_2$  regularization strength  
649 were varied. In all cases, the primary optimisation criterion was the F1-score of  
650 the chimeric class, averaged across folds.

651 For each model family, the hyperparameter configuration with the highest  
652 mean cross-validation F1-score was selected as the best-tuned estimator. These  
653 tuned models were then refitted on the full training set and evaluated once on the  
654 held-out test set to obtain unbiased estimates of performance. Test-set metrics in-  
655 cluded accuracy, precision, recall, F1-score for the chimeric class, and ROC–AUC.  
656 Confusion matrices and ROC curves were generated for the top-performing mod-  
657 els to characterise common error modes, such as false negatives (missed chimeric  
658 reads) and false positives (clean reads incorrectly labelled as chimeric). The final  
659 model or small set of models for downstream interpretation was chosen based on  
660 a combination of test-set F1-score, ROC–AUC, and practical considerations such  
661 as model complexity and ease of deployment within a feature extraction pipeline.

### 662 3.1.5 Feature Importance and Interpretation

663 To relate model decisions to biologically meaningful signals, feature-importance  
664 analyses were performed on the best-performing tree-based models. Two comple-  
665 mentary approaches were used. First, built-in importance measures from ensemble  
666 methods (e.g., split-based importances in Random Forest and Gradient Boosting)  
667 were examined to obtain an initial ranking of features based on their contribution  
668 to reducing impurity. Second, model-agnostic permutation importance was com-  
669 puted on the test set by repeatedly permuting each feature column while keeping  
670 all others fixed and measuring the resulting decrease in F1-score. Features whose

671 permutation led to a larger performance drop were interpreted as more influential  
672 for chimera detection.

673 For interpretability, individual features were grouped into four conceptual  
674 families: (i) supplementary alignment and alignment-structure features (e.g., SA  
675 count, spacing between alignment segments, strand consistency), (ii) CIGAR-  
676 derived soft-clipping features (e.g., left and right soft-clipped length, total clipped  
677 bases), (iii) k-mer composition discontinuity features (e.g., cosine distance and  
678 Jensen–Shannon divergence between k-mer profiles of read segments), and (iv) mi-  
679 crohomology descriptors (e.g., microhomology length and local GC content around  
680 putative breakpoints). Aggregating permutation importance scores within each  
681 family allowed assessment of which biological signatures contributed most strongly  
682 to the classifier’s performance. This analysis provided a basis for interpreting the  
683 trained models in terms of known mechanisms of PCR-induced template switching  
684 and for identifying which alignment- and sequence-derived cues are most informa-  
685 tive for distinguishing chimeric from clean mitochondrial reads.

### 686 3.1.6 Validation and Testing

687 Validation will involve both internal and external evaluations. Internal valida-  
688 tion was achieved through five-fold cross-validation on the training data to verify  
689 model generalization and reduce variance due to random sampling. External vali-  
690 dation will be achieved through testing on the 20% hold-out dataset derived from  
691 the simulated reads, which will be an unbiased benchmark to evaluate how well  
692 the trained models generalized to unseen data. All feature extraction and prepro-  
693 cessing steps were performed using the same feature extraction pipeline to ensure

694 consistency and comparability across validation stages.

695 Comparative evaluation was performed across all candidate algorithms, in-  
696 cluding a trivial dummy classifier, L2-regularized logistic regression, a calibrated  
697 linear SVM, k-nearest neighbours, Gaussian Naïve Bayes, decision-tree ensembles,  
698 gradient boosting methods, and a shallow MLP. This evaluation determined which  
699 models demonstrated the highest predictive performance and computational effi-  
700 ciency under identical data conditions. Their metrics were compared to identify  
701 which algorithms were most suitable for further refinement.

### 702 **3.1.7 Documentation**

703 Comprehensive documentation was maintained throughout the study to ensure  
704 transparency and reproducibility. All stages of the research, including data gath-  
705 ering, preprocessing, feature extraction, model training, and validation, were sys-  
706 tematically recorded in a `.README` file in the GitHub repository. For each ana-  
707 lytical step, the corresponding parameters, software versions, and command line  
708 scripts were documented to enable exact replication of results.

709 The repository structure followed standard research data management prac-  
710 tices, with clear directories for datasets and scripts. Computational environments  
711 were standardized using Conda, with an environment file (`environment.arm.yml`)  
712 specifying dependencies and package versions to maintain consistency across sys-  
713 tems.

714 For manuscript preparation and supplementary materials, Overleaf (L<sup>A</sup>T<sub>E</sub>X)  
715 was used to produce publication-quality formatting and consistent referencing. f

## <sup>716</sup> 3.2 Calendar of Activities

<sup>717</sup> Table 3.1 presents the project timeline in the form of a Gantt chart, where each  
<sup>718</sup> bullet point corresponds to approximately one week of planned activity.

Table 3.1: Timetable of Activities

Activities (2025)	Nov	Dec	Jan	Feb	Mar	Apr	May
Data Collection and Simulation	• • •						
Feature Extraction Pipeline	• •	•					
Machine Learning Development			• •	• • •	• • •	• •	
Testing and Validation						• •	• • •
Documentation	• • •	• • •	• • •	• • •	• • •	• • •	• • •

719 **Chapter 4**

720 **Results and Discussion**

721 **4.1 Descriptive Analysis of Features**

722 This chapter presents the performance of the proposed feature set and machine-  
723 learning models for detecting PCR-induced chimeric reads in simulated mitochon-  
724 drial Illumina data. We first describe the behaviour of the main features, then  
725 compare baseline classifiers, assess the effect of hyperparameter tuning, and fi-  
726 nally analyse feature importance in terms of individual variables and biologically  
727 motivated feature families.

728 The final dataset contained 31,986 reads for training and 7,997 reads for test-  
729 ing, with classes balanced (approximately 4,000 clean and 4,000 chimeric reads in  
730 the test split).

### 731 4.1.1 Univariate Distributions

732 The kernel density plots in Figures 4.1a–4.1f collectively show that alignment-  
733 based features provide the strongest separation between clean and chimeric reads.  
734 The distribution of `sa_count` (Figure 4.1a) is distinctly bimodal, with clean reads  
735 concentrated near zero and chimeric reads peaking around one, reflecting the  
736 frequent presence of supplementary alignments in chimeras. A similar pattern of  
737 clear separation is observed in `softclip_left` and `softclip_right` (Figures 4.1c  
738 and 4.1d), where clean reads cluster tightly at zero while chimeric reads display  
739 broad, long-tailed distributions, consistent with extensive soft clipping when  
740 a read spans multiple genomic locations. In contrast, `microhomology_length`  
741 (Figure 4.1b) shows substantial overlap between classes, with both distribu-  
742 tions sharply concentrated near zero and exhibiting smaller secondary peaks  
743 at short integer lengths, indicating limited discriminative value under the sim-  
744 ulated conditions. Finally, the k-mer-based features `kmer_js_divergence` and  
745 `kmer_cosine_diff` (Figures 4.1e and 4.1f) exhibit highly overlapping, multimodal  
746 distributions with both classes peaking near 1.0; although chimeric reads appear  
747 slightly less concentrated at the highest similarity values, the separation is weak  
748 overall.

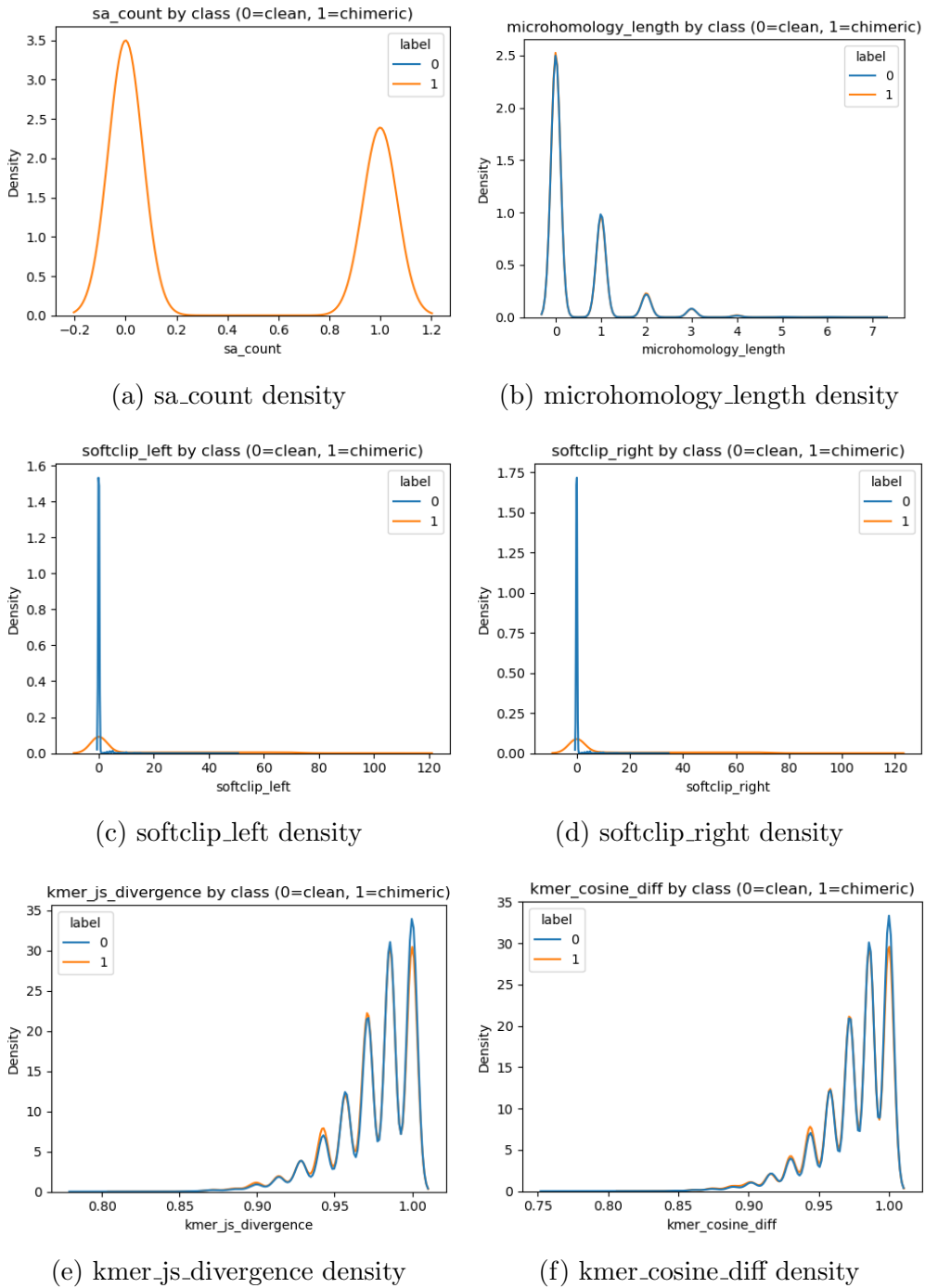


Figure 4.1: Kernel density plots of six key features comparing clean and chimeric reads.

## 749 4.2 Baseline Classification Performance

750 Table 4.1 summarises the performance of eleven classifiers trained on the engi-  
751 neered feature set using five-fold cross-validation and evaluated on the held-out  
752 test set. All models were optimised using default hyperparameters, without ded-  
753 icated tuning.

754 The dummy baseline, which always predicts the same class regardless of the  
755 input features, achieved an accuracy of 0.50 and test F1-score of 0.67. This re-  
756 flects the balanced class distribution and provides a lower bound for meaningful  
757 performance.

758 Across other models, test F1-scores clustered in a narrow band between ap-  
759 proximately 0.74 and 0.77 and ROC–AUC values between 0.82 and 0.84. Gradi-  
760 ent boosting, CatBoost, LightGBM, XGBoost, bagging trees, random forest, and  
761 multilayer perceptron (MLP) all produced very similar scores, with CatBoost and  
762 gradient boosting slightly ahead (test F1  $\approx$  0.77, ROC–AUC  $\approx$  0.84). Linear  
763 models (logistic regression and calibrated linear SVM) performed only marginally  
764 worse (test F1  $\approx$  0.74), while Gaussian Naive Bayes lagged behind with substan-  
765 tially lower F1 ( $\approx$  0.65) despite very high precision for the chimeric class.

Table 4.1: Performance of baseline classifiers on the held-out test set.

model	test_accuracy	test_precision	test_recall	test_f1	test_roc_auc
dummy_baseline	0.500000	0.500000	1.000000	0.667000	0.500000
logreg_l2	0.789000	0.945000	0.614000	0.744000	0.821000
linear_svm_calibrated	0.789000	0.945000	0.614000	0.744000	0.820000
random_forest	0.788000	0.894000	0.654000	0.755000	0.834000
extra_trees	0.788000	0.901000	0.647000	0.753000	0.824000
gradient_boosting	0.802000	0.936000	0.648000	0.766000	0.840000
xgboost	0.800000	0.929000	0.650000	0.765000	0.839000
lightgbm	0.799000	0.926000	0.650000	0.764000	0.838000
catboost	0.803000	0.936000	0.650000	0.767000	0.839000
knn	0.782000	0.892000	0.642000	0.747000	0.815000
gaussian_nb	0.741000	0.996000	0.483000	0.651000	0.819000
bagging_trees	0.792000	0.900000	0.657000	0.760000	0.837000
mlp	0.789000	0.931000	0.625000	0.748000	0.819000

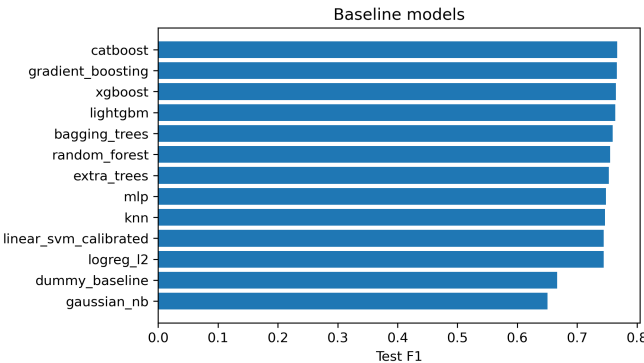


Figure 4.2: Test F1 of all baseline classifiers, showing that no single model clearly dominates and several achieve comparable performance.

### 766 4.3 Effect of Hyperparameter Tuning

767 To assess whether performance could be improved further, ten model families un-  
 768 derwent randomised hyperparameter search (Chapter 3). The tuned metrics are  
 769 summarised in Table 4.2. Overall, tuning yielded modest but consistent gains for  
 770 tree-based ensembles and boosting methods, while leaving linear models essen-

771 tially unchanged or slightly worse.

772 CatBoost, gradient boosting, LightGBM, XGBoost, random forest, bagging  
773 trees, and MLP all experienced small increases in test F1 (typically  $\Delta F1 \approx 0.002 -$   
774 0.009) and ROC–AUC (up to  $\Delta AUC \approx 0.008$ ). After tuning, CatBoost remained  
775 the best performer with test accuracy 0.802, precision 0.924, recall 0.658, F1-score  
776 0.769, and ROC–AUC 0.844. Gradient boosting achieved almost identical perfor-  
777 mance (F1 0.767, AUC 0.843). Random forest and bagging trees also improved  
778 to F1 scores around 0.763 with AUC  $\approx 0.842$ .

Table 4.2: Performance of tuned classifiers on the held-out test set.

model	test_accuracy	test_precision	test_recall	test_f1	test_roc_auc
logreg_l2_tuned	0.788000	0.946000	0.612000	0.743000	0.818000
linear_svm_calibrated_tuned	0.788000	0.944000	0.612000	0.743000	0.818000
random_forest_tuned	0.797000	0.915000	0.655000	0.763000	0.842000
extra_trees_tuned	0.794000	0.910000	0.652000	0.760000	0.837000
gradient_boosting_tuned	0.802000	0.928000	0.654000	0.767000	0.843000
xgboost_tuned	0.799000	0.922000	0.653000	0.765000	0.839000
lightgbm_tuned	0.801000	0.930000	0.651000	0.766000	0.842000
catboost_tuned	0.802000	0.924000	0.658000	0.769000	0.844000
bagging_trees_tuned	0.798000	0.922000	0.650000	0.763000	0.842000
mlp_tuned	0.790000	0.934000	0.625000	0.749000	0.821000

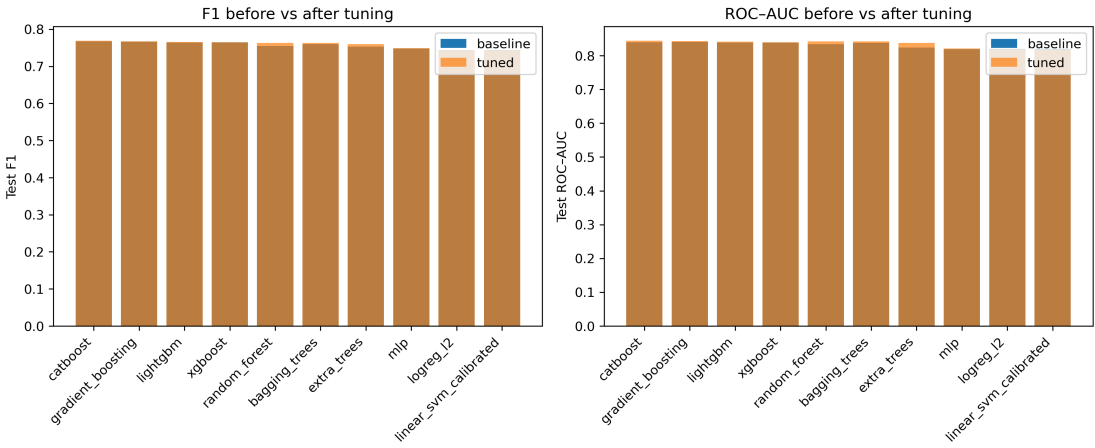


Figure 4.3: Comparison of test F1 (left) and ROC–AUC (right) for baseline and tuned models. Hyperparameter tuning yields small but consistent gains, particularly for tree-based ensembles.

779 Because improvements are small and within cross-validation variability, we  
 780 interpret tuning as stabilising and slightly refining the models rather than funda-  
 781 mentally altering their behaviour or their relative ranking.

## 782 4.4 Detailed Evaluation of Representative Mod- 783 els

784 For interpretability and diversity, four tuned models were selected for deeper  
 785 analysis: CatBoost (best-performing boosted tree), scikit-learn gradient boost-  
 786 ing (canonical gradient-boosting implementation), random forest (non-boosted  
 787 ensemble baseline), and L2-regularised logistic regression (linear baseline). All  
 788 models were trained on the engineered feature set and evaluated on the same  
 789 held-out test data.

#### 790 4.4.1 Confusion Matrices and Error Patterns

791 Classification reports and confusion matrices for the four models reveal consistent  
792 patterns. CatBoost and gradient boosting both reached overall accuracy of ap-  
793 proximately 0.80 with similar macro-averaged F1 scores ( $\sim 0.80$ ). For CatBoost,  
794 precision and recall for clean reads were 0.73 and 0.95, respectively, while for  
795 chimeric reads they were 0.92 and 0.66 (F1 = 0.77). Gradient boosting showed  
796 nearly identical trade-offs.

797 Random forest attained slightly lower accuracy (0.80) and chimeric F1 (0.76),  
798 whereas logistic regression achieved the lowest accuracy among the four (0.79)  
799 and chimeric F1 (0.74), although it provided the highest chimeric precision (0.95)  
800 at the cost of lower recall (0.61).

801 Across all models, errors were asymmetric. False negatives (chimeric reads  
802 predicted as clean) were more frequent than false positives. For example, CatBoost  
803 misclassified 1 369 chimeric reads as clean but only 215 clean reads as chimeric.  
804 This pattern indicates that the models are conservative: they prioritise avoiding  
805 spurious chimera calls at the expense of missing some true chimeras. Depending on  
806 downstream application, alternative decision thresholds or cost-sensitive training  
807 could be explored to adjust this balance.

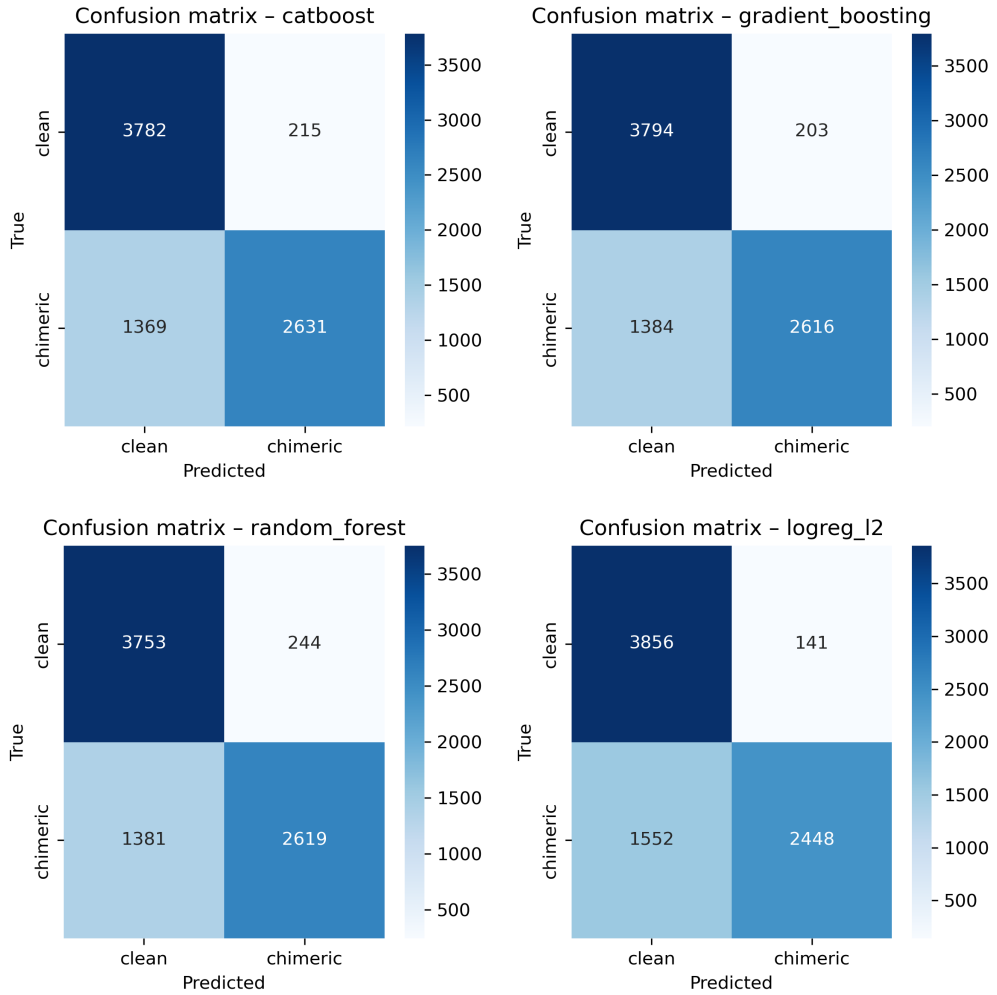


Figure 4.4: Confusion matrices for the four representative models on the held-out test set. All models show more false negatives (chimeric reads called clean) than false positives.

#### 808 4.4.2 ROC and Precision–Recall Curves

809 Receiver operating characteristic (ROC) and precision–recall (PR) curves (Figure 4.5) further support the similarity among the top models. The three tree-based  
 810 ensembles (CatBoost, gradient boosting, random forest) achieved ROC–AUC val-  
 811 ues of approximately 0.84 and average precision (AP) around 0.88. Logistic re-  
 812

813 gression performed slightly worse ( $AUC \approx 0.82$ ,  $AP \approx 0.87$ ) but still substantially  
814 better than random guessing.

815 The PR curves show that precision remains above 0.9 across a broad range  
816 of recall values (up to roughly 0.5–0.6), after which precision gradually declines.  
817 This behaviour indicates that the models can assign very high confidence to a  
818 subset of chimeric reads, while more ambiguous reads can only be recovered by  
819 accepting lower precision.

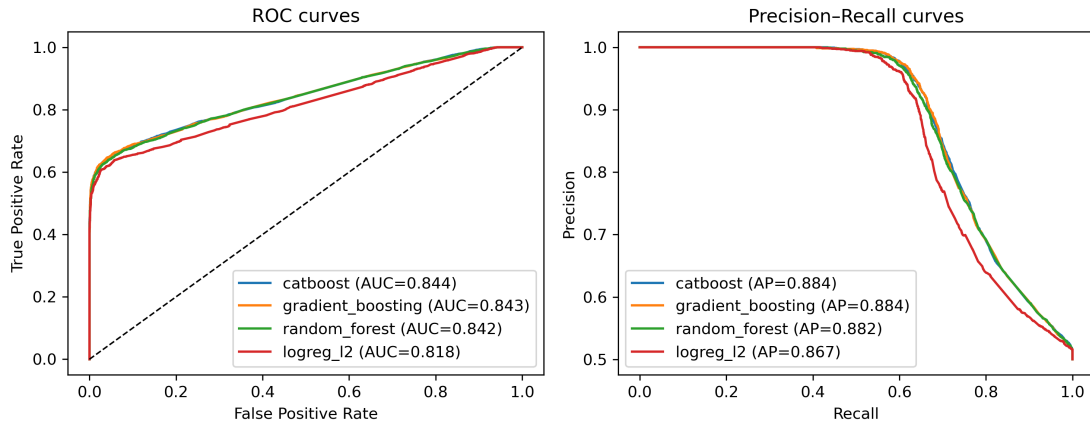


Figure 4.5: ROC (left) and precision–recall (right) curves for the four representative models on the held-out test set. Tree-based ensembles cluster closely, with logistic regression performing slightly but consistently worse.

820    **4.5 Feature Importance and Biological Interpre-**  
821    **tation**

822    **4.5.1 Permutation Importance of Individual Features**

823    To understand how each classifier made predictions, feature importance was quan-  
824    tified using permutation importance. In this approach, the values of a single fea-  
825    ture are randomly shuffled, and the resulting drop in  $F_1$  score ( $\Delta F_1$ ) reflects how  
826    strongly the model depends on that feature. Greater decreases in  $F_1$  indicate  
827    stronger reliance on that feature. This analysis was applied to four representa-  
828    tive models: CatBoost, Gradient Boosting, Random Forest, and  $L_2$ -regularized  
829    Logistic Regression.

830       As shown in Figure 4.6, the total number of clipped bases consistently pro-  
831    vides a strong predictive signal, particularly in Random Forest, Gradient Boosting,  
832    and  $L_2$ -regularized Logistic Regression. CatBoost differs by assigning the highest  
833    importance to k-mer divergence metrics such as `kmer_js_divergence`, which cap-  
834    ture subtle sequence changes resulting from structural variants or PCR-induced  
835    chimeras. Soft-clipping features (`softclip_left` and `softclip_right`) provide  
836    additional context around breakpoints, complementing these primary signals in  
837    all models except Gradient Boosting.  $L_2$ -regularized Logistic Regression relies  
838    more on alignment-based split-read metrics when breakpoints are simple, but it is  
839    less effective at detecting complex rearrangements that introduce novel sequences.

840       Overall, these results indicate that accurate detection of chimeric reads relies  
841    on both alignment-based signals and k-mer compositional information. Explicit

842 microhomology features contribute minimally in this analysis, and combining both  
 843 alignment-based and sequence-level features enhances model sensitivity and speci-  
 844 ficity.

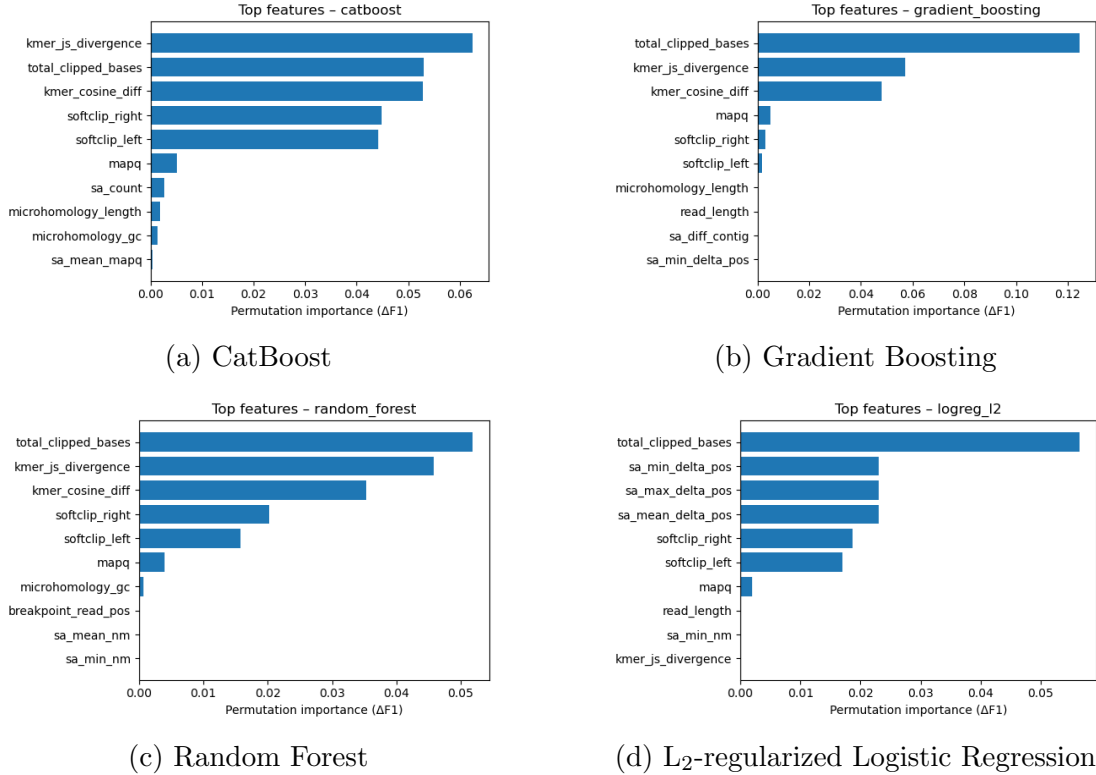


Figure 4.6: Permutation-based feature importance for four representative classifiers. Clipping and k-mer composition features are generally the strongest predictors, whereas microhomology and other alignment metrics contribute minimally.

### 845 4.5.2 Feature Family Importance

846 To evaluate the contribution of broader biological signals, features were  
 847 grouped into five families: SA\_structure (supplementary alignment and seg-  
 848 ment metrics, e.g., has\_sa, sa\_count, sa\_min\_delta\_pos, sa\_mean\_nm), Clipping  
 849 (softclip\_left, softclip\_right, total\_clipped\_bases, breakpoint\_read\_pos),

850 Kmer\_jump (`kmer_cosine_diff`, `kmer_js_divergence`), Micro\_homology, and  
851 Other (e.g., `mapq`).

852 Aggregated analyses reveal consistent patterns across models. In CatBoost,  
853 the Clipping family has the largest cumulative contribution (0.14), followed  
854 by Kmer\_jump (0.12), with Other features contributing modestly (0.005) and  
855 SA\_structure (0.003) and Micro\_homology (0.003) providing minimal predictive  
856 power. Gradient Boosting shows a similar trend, with Clipping (0.13) domi-  
857 nating, Kmer\_jump (0.11) secondary, and the remaining families contributing  
858 negligibly. Random Forest integrates both Clipping (0.088) and Kmer\_jump  
859 (0.08) effectively, while SA\_structure, Micro\_homology, and Other remain minor  
860 contributors. L<sub>2</sub>-regularized Logistic Regression emphasizes Clipping (0.09)  
861 and SA\_structure (0.07), with Kmer\_jump and Micro\_homology having minimal  
862 impact.

863 Both feature-level and aggregated analyses indicate that detection of chimeric  
864 reads in this dataset relies primarily on alignment disruptions (Clipping) and  
865 k-mer compositional shifts (Kmer\_jump), which often arise from PCR-induced  
866 recombination events, while explicit microhomology features contribute minimally.

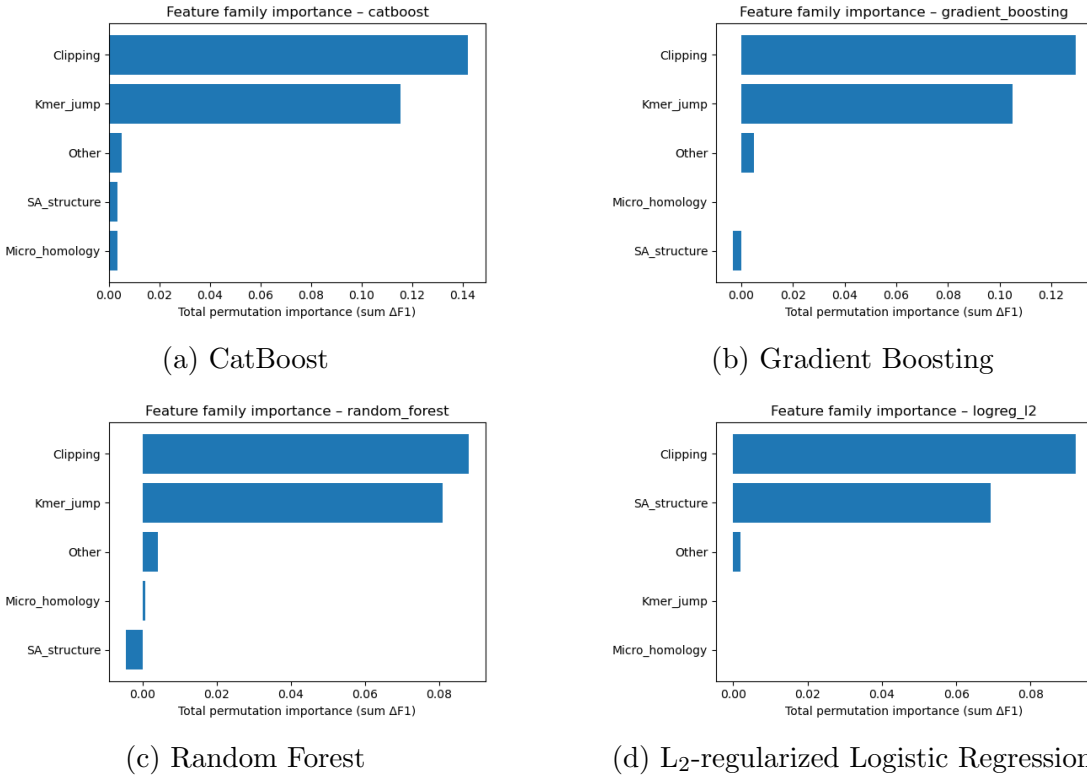


Figure 4.7: Aggregated feature family importance across four models. Clipping and k-mer compositional shifts are consistently the dominant contributors, while SA\_structure, Micro\_homology, and other features contribute minimally.

## 867 4.6 Summary of Findings

868 After removing trivially discriminative metadata, all models performed substan-  
 869 tially better than the dummy baseline, with test F1-scores around 0.76 and ROC-  
 870 AUC values near 0.84. Hyperparameter tuning yielded modest improvements,  
 871 with boosting methods, particularly CatBoost and gradient boosting, achieving  
 872 the highest performance. Confusion matrices and precision-recall curves indicate  
 873 that these models prioritise precision for chimeric reads while accepting lower re-  
 874 call, which a conservative strategy appropriate for scenarios where false positives

875 are costly.

876 Feature importance analyses revealed that alignment disruptions, such as clip-  
877 ping, and abrupt k-mer composition changes accounted for most predictive power.  
878 In contrast, microhomology metrics and supplementary alignment descriptors con-  
879 tributed minimally. These results indicate that features based on read alignment  
880 and k-mer composition are sufficient to train classifiers for detecting mitochon-  
881 drial PCR-induced chimera reads, without needing additional quality-score or  
882 positional information in the conditions tested.

# <sup>883</sup> References

- <sup>884</sup> Anderson, S., Bankier, A., Barrell, B., Bruijn, M., Coulson, A., Drouin, J., ...  
<sup>885</sup> Young, I. (1981, 04). Sequence and organization of the human mitochondrial  
<sup>886</sup> genome. *Nature*, *290*, 457-465. doi: 10.1038/290457a0
- <sup>887</sup> Arango, G., Garner, E., Pruden, A., Heath, L., Vikesland, P., & Zhang, L. (2018,  
<sup>888</sup> 02). Deeparg: A deep learning approach for predicting antibiotic resistance  
<sup>889</sup> genes from metagenomic data. *Microbiome*, *6*. doi: 10.1186/s40168-018  
<sup>890</sup> -0401-z
- <sup>891</sup> Bentley, D. R., Balasubramanian, S., Swerdlow, H. P., Smith, G. P., Milton, J.,  
<sup>892</sup> Brown, C. G., ... Smith, A. J. (2008). Accurate whole human genome  
<sup>893</sup> sequencing using reversible terminator chemistry. *Nature*, *456*(7218), 53–  
<sup>894</sup> 59. doi: 10.1038/nature07517
- <sup>895</sup> Boore, J. L. (1999). Animal mitochondrial genomes. *Nucleic Acids Research*,  
<sup>896</sup> *27*(8), 1767–1780. doi: 10.1093/nar/27.8.1767
- <sup>897</sup> Cameron, S. L. (2014). Insect mitochondrial genomics: Implications for evolution  
<sup>898</sup> and phylogeny. *Annual Review of Entomology*, *59*, 95–117. doi: 10.1146/  
<sup>899</sup> annurev-ento-011613-162007
- <sup>900</sup> Dierckxsens, N., Mardulyn, P., & Smits, G. (2017). Novoplasty: de novo assembly  
<sup>901</sup> of organelle genomes from whole genome data. *Nucleic Acids Research*,

- 902            45(4), e18. doi: 10.1093/nar/gkw955
- 903    Edgar, R. C. (2016). Uchime2: improved chimera prediction for amplicon se-  
904        quencing. *bioRxiv*. Retrieved from <https://api.semanticscholar.org/>  
905        CorpusID:88955007
- 906    Edgar, R. C. (n.d.). *Uchime in practice*. Retrieved from [https://www.drive5.com/usearch/manual7/uchime\\_practical.html](https://www.drive5.com/usearch/manual7/uchime_practical.html)
- 907    Edgar, R. C., Haas, B. J., Clemente, J. C., Quince, C., & Knight, R. (2011).  
908        Uchime improves sensitivity and speed of chimera detection. *Bioinformatics*,  
909        27(16), 2194–2200. doi: 10.1093/bioinformatics/btr381
- 910    Glenn, T. C. (2011). Field guide to next-generation dna sequencers. *Molecular  
911        Ecology Resources*, 11(5), 759–769. doi: 10.1111/j.1755-0998.2011.03024.x
- 912    Gonzalez, J. M., Zimmermann, J., & Saiz-Jimenez, C. (2004, 09). Evalu-  
913        ating putative chimeric sequences from pcr-amplified products. *Bioin-  
914        formatics*, 21(3), 333-337. Retrieved from <https://doi.org/10.1093/bioinformatics/bti008>  
915        doi: 10.1093/bioinformatics/bti008
- 916    Gray, M. W. (2012). Mitochondrial evolution. *Cold Spring Harbor perspectives  
917        in biology*, 4. Retrieved from <https://doi.org/10.1101/cshperspect.a011403>  
918        doi: 10.1101/cshperspect.a011403
- 919    Hahn, C., Bachmann, L., & Chevreux, B. (2013). Reconstructing mitochondrial  
920        genomes directly from genomic next-generation sequencing reads—a baiting  
921        and iterative mapping approach. *Nucleic Acids Research*, 41(13), e129. doi:  
922        10.1093/nar/gkt371
- 923    Jin, J.-J., Yu, W.-B., Yang, J., Song, Y., dePamphilis, C. W., Yi, T.-S., & Li,  
924        D.-Z. (2020). Getorganelle: a fast and versatile toolkit for accurate de  
925        novo assembly of organelle genomes. *Genome Biology*, 21(1), 241. doi:  
926        10.1186/s13059-020-02154-5  
927

- 928 Judo, M. S. B., Wedel, W. R., & Wilson, B. H. (1998). Stimulation and sup-  
929 pression of pcr-mediated recombination. *Nucleic Acids Research*, *26*(7),  
930 1819–1825. doi: 10.1093/nar/26.7.1819
- 931 Labrador, K., Agmata, A., Palermo, J. D., Ravago-Gotanco, R., & Pante, M. J.  
932 (2021). Mitochondrial dna reveals genetically structured haplogroups of  
933 bali sardinella (sardinella lemuru) in philippine waters. *Regional Studies in*  
934 *Marine Science*, *41*, 101588. doi: 10.1016/j.rsma.2020.101588
- 935 Li, H. (2018, 05). Minimap2: pairwise alignment for nucleotide sequences. *Bioin-*  
936 *formatics*, *34*(18), 3094-3100. Retrieved from <https://doi.org/10.1093/bioinformatics/bty191>  
937 doi: 10.1093/bioinformatics/bty191
- 938 Liang, Q., Bible, P. W., Liu, Y., Zou, B., & Wei, L. (2020, 02). Deepmi-  
939 crobes: taxonomic classification for metagenomics with deep learning. *NAR*  
940 *Genomics and Bioinformatics*, *2*(1), lqaa009. Retrieved from <https://doi.org/10.1093/nargab/lqaa009> doi: 10.1093/nargab/lqaa009
- 941 Metzker, M. L. (2010). Sequencing technologies — the next generation. *Nature*  
942 *Reviews Genetics*, *11*(1), 31–46. doi: 10.1038/nrg2626
- 943 Mysara, M., Saeys, Y., Leys, N., Raes, J., & Monsieurs, P. (2015). Catch,  
944 an ensemble classifier for chimera detection in 16s rrna sequencing stud-  
945 ies. *Applied and Environmental Microbiology*, *81*(5), 1573-1584. Retrieved  
946 from <https://journals.asm.org/doi/abs/10.1128/aem.02896-14> doi:  
947 10.1128/AEM.02896-14
- 948 Peccoud, J., Lequime, S., Moltini-Conclois, I., Giraud, I., Lambrechts, L., &  
949 Gilbert, C. (2018, 04). A survey of virus recombination uncovers canon-  
950 ical features of artificial chimeras generated during deep sequencing li-  
951 brary preparation. *G3 Genes—Genomes—Genetics*, *8*(4), 1129-1138. Re-  
952 trieved from <https://doi.org/10.1534/g3.117.300468> doi: 10.1534/

- 954 g3.117.300468
- 955 Qin, Y., Wu, L., Zhang, Q., Wen, C., Nostrand, J. D. V., Ning, D., ... Zhou, J.  
956 (2023). Effects of error, chimera, bias, and gc content on the accuracy of  
957 amplicon sequencing. *mSystems*, 8(6), e01025-23. Retrieved from <https://journals.asm.org/doi/abs/10.1128/msystems.01025-23> doi: 10.1128/  
958 msystems.01025-23
- 959
- 960 Qiu, X., Wu, L., Huang, H., McDonel, P. E., Palumbo, A. V., Tiedje, J. M., &  
961 Zhou, J. (2001). Evaluation of pcr-generated chimeras, mutations, and het-  
962 eroduplexes with 16s rrna gene-based cloning. *Applied and Environmental*  
963 *Microbiology*, 67(2), 880–887. doi: 10.1128/AEM.67.2.880-887.2001
- 964 Ren, J., Song, K., Deng, C., Ahlgren, N., Fuhrman, J., Li, Y., ... Sun, F. (2020,  
965 01). Identifying viruses from metagenomic data using deep learning. *Quan-*  
966 *titative Biology*, 8. doi: 10.1007/s40484-019-0187-4
- 967 Rodriguez-Martin, B., Palumbo, E., Marco-Sola, S., Griebel, T., Ribeca, P.,  
968 Alonso, G., ... Djebali, S. (2017, 01). Chimpipe: Accurate detection of  
969 fusion genes and transcription-induced chimeras from rna-seq data. *BMC*  
970 *Genomics*, 18. doi: 10.1186/s12864-016-3404-9
- 971 Rognes, T., Flouri, T., Nichols, B., Quince, C., & Mahé, F. (2016). Vsearch: a  
972 versatile open source tool for metagenomics. *PeerJ*, 4, e2584. doi: 10.7717/  
973 peerj.2584
- 974 Sedlazeck, F., Rescheneder, P., Smolka, M., Fang, H., Nattestad, M., von Haeseler,  
975 A., & Schatz, M. (2018, 06). Accurate detection of complex structural  
976 variations using single-molecule sequencing. *Nature Methods*, 15. doi: 10  
977 .1038/s41592-018-0001-7
- 978 Sfeir, A., & Symington, L. S. (2015). Microhomology-mediated end joining: A  
979 back-up survival mechanism or dedicated pathway? *Trends in Biochemical*

- 980        *Sciences*, 40(11), 701-714. Retrieved from <https://www.sciencedirect.com/science/article/pii/S0968000415001589> doi: <https://doi.org/10.1016/j.tibs.2015.08.006>
- 981
- 982
- 983        Vervier, K., Mahé, P., Tournoud, M., Veyrieras, J.-B., & Vert, J.-P. (2015,  
984        11). Large-scale machine learning for metagenomics sequence classifica-  
985        tion. *Bioinformatics*, 32(7), 1023-1032. Retrieved from <https://doi.org/10.1093/bioinformatics/btv683> doi: 10.1093/bioinformatics/btv683
- 986
- 987        Willette, D., Bognot, E., Mutia, M. T., & Santos, M. (2011). *Biology and ecology  
988        of sardines in the philippines: A review* (Vol. 13; Tech. Rep. No. 1). NFRDI  
989        Technical Paper Series. Retrieved from <https://nfrdi.da.gov.ph/tpjf/etc/Willette%20et%20al.%20Sardines%20Review.pdf>
- 990